AD-A040 692   STANFORD UNIV CALIF CENTER FOR MATERIALS RESEARCH   F/G 20/2
                CONTROL OF IMPURITIES IN THE EPITAXIAL GROWTH OF HIGH QUALITY G--ETC(U)
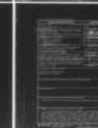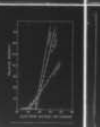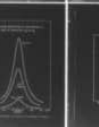   MAY 77   D A STEVENSON, B L MATTES, H DUN   N00014-75-C-0887
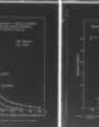UNCLASSIFIED   CMR-77-4   NL
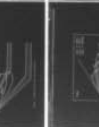
1 OF 1
AD
A040692

END

DATE
FILMED
7-77

ADA040692

DDC

JUN 20 1977

B

CENTER FOR MATERIALS RESEARCH

STANFORD UNIVERSITY • STANFORD, CALIFORNIA

May 1977   Technical Report   CMR-77-4

CONTROL OF IMPURITIES IN THE EPITAXIAL GROWTH

OF HIGH QUALITY GaAs

Response of the Molecular Beam-Mass Spectrometer

Analysis and Calibration

Sponsored by the

Physical Sciences Division of the

Office of Naval Research

Contract No. N00014-75-C-0887 New

Principal Investigator:

Professor David A. Stevenson
Department of Materials Science and Engineering

Research Associate:

Brenton L. Mattes
Center for Materials Research

Research Assistant:

Haiping Dun
Department of Materials Science and Engineering

Center for Materials Research
Stanford University
Stanford, CA. 94305

Reproduction in whole or in part is permitted for
any purpose of the United States Government.

ABSTRACT

A molecular beam-mass spectrometer (MBMS) has been developed
to sample ambient gas atmospheres in epitaxial growth systems at high
temperatures and at atmospheric pressure. At present the MBMS is
capable of analyzing ppm quantities of gaseous species that result from
chemical transport reactions between the ambient H_2 atmosphere and
the growth system components (e.g., fused quartz and graphite). The
MBMS consists of three differentially pumped stages separated by a
nozzle and a skimmer orifice and a detector aperture. The gas is expanded
through the nozzle to establish a supersonic flow region (Mach disc)
which is sampled by the skimmer to develop a well-collimated molecular
beam. The molecular beam is then ionized and detected by a quadrapole
mass analyser. The response and interpretation of the data from the
MBMS are analyzed and discussed to obtain an overall calibration of
the system. The sensitivity for most gaseous species in H_2 at
atmospheric pressure and at $800^{\circ}C$ is better than 1 ppm without chopping
the beam. Initial results indicate that there are ppm levels of Ar,
CO and H_2O in palladium purified H_2. In addition, the formation of
SiO and H_2O by chemical transport reactions between H_2 and fused
quartz at $700^{\circ}C$ and above are in good agreement with existing high
temperature thermodynamic data.

TABLE OF CONTENTS

I. Introduction

A research program is in progress concerning the control and identification of impurities that are incorporated during the liquid phase epitaxial (LPE) growth of GaAs. Chemical transport reactions which involve the interaction between the ambient gas atmosphere and the growth system components are a major source for impurities during the growth of epitaxial layers. These reactions, however, are not well characterized and/or controlled at present. In order to obtain more information on these reactions, we have developed a molecular beam-mass spectrometer (MBMS) system capable of analyzing ppm quantities of gaseous species in a high temperature-atmospheric pressure growth system.

The analysis of ambient partial pressures of gases at elevated temperatures, with total pressures on the order of one atmosphere, is of broad interest for many practical systems. Mass spectrometry provides a sensitive method for detecting the masses of gas molecules and their fragments that enter the detection chamber. For high temperature-atmospheric pressure systems, however, one must transport a representative sample of the gas from the environment in question to the detection chamber, which is typically at a pressure of 10^{-8} Torr. This is accomplished by leaking the sample gas into the detection chamber, however, this must be achieved in such a manner that the sample gas is not perturbed by condensation, interaction amongst the gaseous species or interaction between the gaseous species and the walls of the apparatus. To accomplish this objective, the gas is sampled with a carefully designed series of orifices and chambers that are differentially pumped

1

so that a well-defined molecular beam of the sample gas is formed. The objective is to transmit this beam directly to the detection chamber, with no intermediate interaction with the walls or other gas molecules.

II. Description and Operation of the Molecular Beam Spectrometer

The present design of the MBMS consists of three orifices--the nozzle, the skimmer and the detector aperture--that separate three differentially pumped chambers maintained at pressures of $\sim 10^{-3}$, $\sim 10^{-5}$ and $\sim 10^{-8}$ Torr, respectively (Figure 1). Details for each stage of its operation are described in the following sections.

A. Flow pattern in the first stage nozzle expansion chamber

A supersonic molecular beam can be formed when gas molecules at atmospheric pressure expand through a nozzle orifice into a vacuum. For our system the orifice diameter is 3.2 mils which gives a hydrogen flow rate of ~ 0.2 ℓ/min at room temperature. This has a negligible effect on the 1.2 ℓ/min flow rate inside the furnace. After the gas passes through the nozzle orifice, the mass flow velocity continues to increase along the axis of expansion into the vacuum. The thermal velocity of the gas molecules, on the other hand, is reduced as the molecular beam is collimated. The expansion will stop when the gas molecular density reaches that of the background gases and beyond this region the flow becomes unstable. The flow pattern of the supersonic expansion is shown in Figure 2, where the Mach disk at $x = x_m$ gives the starting point of the unstable flow. The background pressure in

2

the expansion chamber is maintained below 5×10^{-3} Torr by a 2400 ℓ/sec diffusion pump. The maximum axial Mach number is greater than 10 which produces a highly collimated molecular beam.

Strictly speaking, the gas expansion is a function not only of the source and background pressure ratio, but also of the mass, temperature and molecular structure of the sampled gas. For example, we have observed that the beam intensity decreases as the furnace is heated and that air collimates better than hydrogen. This effect is shown in Figure 3 where the beam intensity is plotted as a function of its divergent angle θ, which is related to the ratio of the thermal velocity to the mass flow velocity. Thus light molecules expand faster than heavier ones. In addition, as the furnace is heated the gas density in the furnace decreases. This, in addition to a higher thermal velocity, gives a lower beam density. In summary, the optimal position of the skimmer orifice (Section II-B) on the axis of the beam depends on the species and the temperature of the gas to be detected. Therefore, the skimmer must be positioned close to the nozzle in the Mach disc region to maintain a high beam density in the second stage for high temperatures and light gases. For heavier gases at room temperature, the skimmer must be located further downstream of the nozzle throat to avoid high pressures in the second stage.

B. Function of the second stage skimmer

The skimmer was designed to separate the molecular beam from the turbulent regions of the first stage and to act as a buffer stage between

the first stage nozzle expansion chamber and the third stage detection chamber. The operating pressure in the second stage skimmer chamber is 1.6×10^{-5} Torr which gives a hydrogen molecular mean-free path length of 220 inches (4 times the distance between the skimmer orifice and the detector).

The beam intensity strongly depends on the skimmer's axial and transverse position, as shown in Figures 4 and 5, respectively. The axial operating position was chosen at a nozzle-skimmer distance of 6mm to maintain a pressure of 1.6×10^{-5} Torr in the skimmer chamber. For off-beam operation, the skimmer is positioned 23mm downstream of the nozzle, where the total pressure is only 2% of the beam pressure. In this position the beam spectrum is essentially that of the background. The difference between the on- and off-beam mass spectrum is considered to be the spectrum from the source. The major background gases in the second stage were found to be water and oil vapor at 10^{-8} and 10^{-9} Torr, respectively.

III. <u>System Calibration</u>

The molecular beam-mass spectrometer, in general, is an excellent tool to qualitatively identify gas species, but for quantitative analysis its response is quite complex. Therefore, a very thorough calibration of the system was carried out. The reference used for calibration is based on gas flows through two flow meters, a Brook Instruments R-2-15-B and a Matheson mass-flow meter ALS-30. The former is used to read the H_2 gas flow and the latter is for low flows of N_2 or Ar. In order to

simulate the high purity gas, the gas mixtures were controlled between 100 to 2860 ppm. The primary calibration corrections in the system are related to the mass enhancement in the first stage and the response of the quadrapole mass analyzer.

A. Mass enhancement due to nozzle expansion

As described in Section II-A, the heavier gas molecules are concentrated in the center of the flow, thus enhancing their density. For heavy molecules in a hydrogen carrier gas, the effect is very large. Figure 6 gives the enhancement factor α, defined as the detected signal divided by their flow ratio as a function of the nozzle-skimmer distance. Figures 7a and b give the same plot as a function of the skimmer's transverse position. Clearly, heavy molecules are enhanced on the beam's core and depleted in the peripheral regions.

Four different mechanisms have been proposed to explain the enhancement effect. They are: pressure diffusion[1], free molecular diffusion[2], skimmer induced shock separation[3] and background penetration[4]. From Figure 6 it is seen that the molecular enhancement factor α increases to a maximum downstream from the nozzle throat and then decreases at larger distances. A qualitative explanation of this phenomenon is that the light molecules are always more mobile than the heavy ones, whether in the continuous flow (pressure diffusion) zone or in the free molecular flow (free molecular diffusion) zone. Beyond a certain distance of supersonic expansion, the gas density drops below that of background which causes the light molecules to penetrate into the center of the beam (background penetrating). Hence, the enhancement factor α decreases.

5

Since the experimental results of α versus transverse skimmer position show that the heavy molecules are enriched at the center of the jet and depleted in the peripheral region, the enhancement effect is probably related to molecular diffusion and not skimmer-induced shock separation. If the skimmer-induced shock separation were the major reason for enhancement, heavy molecules would be enriched over the entire flow field and no depleted region would be detected.

A correction factor of 2.6 for N_2 and 4.2 for Ar, based on experiment, must be applied for a skimmer position operated 6mm downstream from the nozzle throat. The correction factors for all the other gases were determined by extrapolation.

B. Corrections for the quadrapole mass analyzer

There are three factors to be considered in using a quadrapole mass analyzer:

1. Ionization Coefficient (I)

Since different molecules have different outer shell electron configurations, the probability of one or more of its electrons to be removed by thermal electrons will be different. The ionization coefficient, in general, is linearly proportional to the number of electrons per molecule[5]. Experimental results are given in Table I.

2. Mass Filter Transmission Coefficient (T)

The light molecules have a better chance to pass through the quadrapole-mass filter than the heavier ones. Values of T are given in Table I.

3. Electron Multiplier Gain (G)

The electron multiplier has a sensitivity proportional to the inverse square root of mass. Values of G are given in Table I.

IV. Interpretation of the Purified Hydrogen Gas Mass Spectrum

Although the relative correction factors have been determined and are summarized in Table I, there are several effects which must be considered to interpret the mass spectrum.

A. Fragmentation patterns

Every gas species has its own fragmentation pattern under thermal electron bombardment. The fragment of methane (CH_4), for example, would be CH_4^+ (100%), CH_3^+ (83%), CH_2^+ (13%), CH^+ (6%) and C^+ (2%). The real quantity of methane is the sum of the signals from all of them. The fragmentation pattern can also be used to identify gas molecular species as well as separating those with the same mass. An example on the separation of the ethane (C_2H_6) signal from mass 28 is given in Appendix I.

B. Ionization potential

Similar to the fragmentation pattern, every molecule, atom or ion has its own ionization potential. If the kinetic energy of the thermal electron is less than the ionization potential of the gas species, then nothing would be detected since no molecule could be ionized. Table II gives several gas molecular ionization potentials compared to those determined experimentally in our MBMS system. Very good agreement is found considering that there is a $\pm$ 0.5 ev error due to the spreading energy of thermal electrons. Figure 8 is an example of how the ionization potentials were determined for mass 28, where hydrogen has a standard ionization potential of 15.4 ev and the nitrogen gas, which was purposely

7

leaked into the system, has an ionization potential of 15.5 ev. The third curve was obtained from an impurity in palladium purified hydrogen at mass 28. An ionization potential of 13.5 ev was observed, which is most likely to be due to CO. The ionization potentials were determined by a linear extrapolation to zero intensity. The ionization potential of hydrogen was used as a reference. The tailing after cut-off is due to thermal energy spreading. Thus, the temperature of the filament should be reduced to increase the accuracy of the measured ionization potential.

C. Hot filament induced reactions

The tungsten filament, which is operated at $2000^{\circ}K$, decomposes the incoming hydrogen molecules to form free atoms with a very high affinity. The decomposed hydrogen atoms in the presence of carbon as an impurity in the filament will react to form methane[6]. Spurious impurity signals from methane, therefore, would be introduced. The proposed chemical reactions are given by:

$$H_2 \overset{2000^{\circ}K}{=} H + H$$

and

$$4H + C(\text{in } W) = CH_4 \ .$$
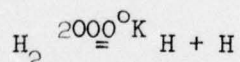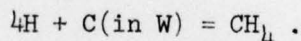
## D. Ion-molecule reactions

The collision of an ion with a molecule will form a stable chemical compound that does not exist in the molecular beam and it is not neutral. For example, H_3^+ could be formed from H_2. The source of the H^+ ion ionized by thermal electron bombardment could be from the incoming gases or from the background gases. Similarly, other species can react

8

and they will appear in the mass spectrum. In our system, fluorine is a major background gas in the detector stage. It is either being desorbed from the vac-ion pump or from the detector unit (we have not been able to account for its presence and it does not appear to be diminished by pumping or bakeouts). When hydrogen is leaked into the detector stage a sudden increase in HF^+ is observed. These and other ion-molecule reactions are summarized below:

$$H^+ + H_2 = H_3^+$$
$$H^+ + F = HF^+$$
$$H^+ + CO = COH^+$$
$$H^+ + N_2 = N_2H^+$$
$$H^+ + Ar = ArH^+ \quad etc.$$
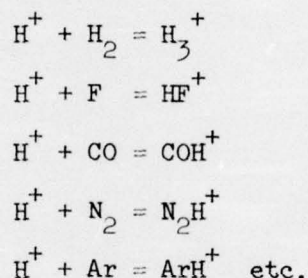
The above reactions show that in an environment of hydrogen, any major impurity peak of mass M will possibly also be accompanied by a small peak at M + 1. This effect has been justified by observing that as the hydrogen pressure is increased there is a decrease in the background signal, e.g., gas F^+ (M = 19) decreases and the corresponding ion molecule signal HF^+ (M = 20) increases.

E. Background gas interference

Background gases, usually from surface desorption, can easily mask the detection of source impurities. For example, when our 3rd stage is well-baked there are certain gaseous species with residual partial pressures of 10^{-10} Torr. Therefore, for a total pressure of

hydrogen at 10^{-6} Torr the limiting sensitivity is 100 ppm. The background gases are usually oil vapor, H_2O, CO, N_2, O_2, etc. Unfortunately, they are also the impurities of most interest in the growth system. The method we have used to minimize background interference without using a molecular beam chopper was mentioned in II-B--the skimmer is moved on and off the beam and the difference in beam intensity is considered to be from impurities in the growth system. This technique increases the sensitivity into the ppm range. There is another effect called bombardment-outgassing that can also produce interference. This occurs when the skimmer is moved from the off to the on-beam position and the total pressure increases by 50 times. The collision frequency between the wall and scattered gases, therefore, will increase by 50 times. This will probably induce more surface gas desorption. In considering all the effects mentioned above, the detected impurity levels in pallidium purified hydrogen to be discussed next should be considered only as an upper limit.

V. Impurities Detected in Palladium Purified Hydrogen and 99.99% Commercial Tank Hydrogen

Figure 9 gives the mass spectrum of palladium purified hydrogen and 99.99% tank hydrogen. The purifier is a new Matheson Model 8362 unit which was He-leak checked. Three major peaks are observed: CH_4 (16), N_2 + CO (28) and Ar (40). The corrected signals, according to Table I, are given in Table II. Quite surprisingly, the impurity level in palladium purified hydrogen is not appreciably lower than

the 99.99% tank hydrogen. The only major difference is for mass 18(H_2O, 28(CO + N_2), 40(Ar) and the others are either too small to be detected or almost the same. As previously discussed, the two larger signals from CH_4 and HF are due to either a hot filament effect or an ion-molecule reaction. The large amount of Ar was not expected, however, it was later found that noble gases are not removed from most commercial gases. In addition, the enhancement factor for Ar is quite large, see II-A. The most important and unexpected result is the large amount of mass 28 in the palladium purified H_2 and in the 99.99% tank hydrogen. Quantitatively, there is at present no way to determine the amount of N_2 or CO. The ionization potential curve in Figure 8, however, shows that there is some CO. If there is CO in the purified hydrogen, the contamination of carbon in the LPE growth of GaAs would be serious even without graphite in the growth system.

VI. Thermodynamic Predictions and High Temperature Gas Analysis

Before going into the details of several possible chemical reactions in the growth system at high temperatures, some general impurity analysis observations were made:

(1) In the growth system, the water vapor content is strongly affected by the system's previous history. Water vapor, for example, is readily adsorbed on the fused quartz surface. For 1.2 ℓ/min purified hydrogen flow, the amount of water vapor could be as high as ~ 500 ppm for new quartz reactor tubes with no prior bakeouts. The water level will drop as the quartz is baked under hydrogen. After several bakeout cycles to 900°C the H_2O level is in the ppm range.

11

This level may be the water vapor in the purified hydrogen. Every time the furnace was exposed to air the water vapor level rose to $\sim$ 50 ppm, which depends on the period of exposure.

(2) Adding a graphite boat to the growth system produced no large increase of methane content at high temperatures. This indicates that the hydrogen-carbon reaction at the graphite surface is very weak, although it is predicted by thermodynamic calculations.

(3) With an arsenic saturated gallium melt in the graphite boat at 900°C, no arsenic or gallium suboxide vapors could be detected. From a thermodynamic analysis $As_2(g)$, $Ga(g)$, $Ga_2O(g)$ would all be less than 1 ppm at 900°C. This level is beyond the present system's detectability.

Returning to a more detailed high temperature analysis of gaseous species in the growth system, we will first look at mass 44 (CO_2 and SiO). This peak showed a relatively large increase at temperatures $> 700^{\circ}$C. Since CO_2 would react with H_2 to form CO and H_2O for temperatures higher than 700°C, the only reasonable explanation for this increase would be the production of SiO. The experimental data for the amount of SiO and H_2O at high temperatures is given in Table IV where the amount of CO_2 was assumed constant. Based on these results the proposed reaction of hydrogen to reduce fused quartz to form water vapor and silicon monoxide happens, i.e..
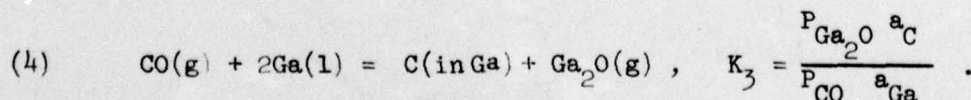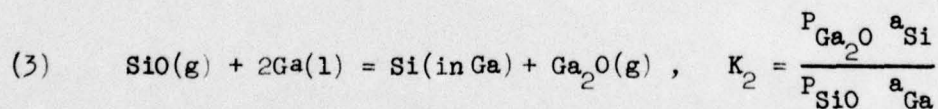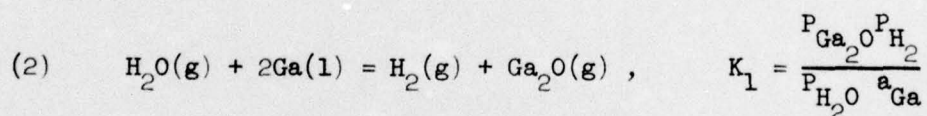
(1) $$H_2(g) + SiO_2(s) = H_2O(g) + SiO(g) \ ,$$
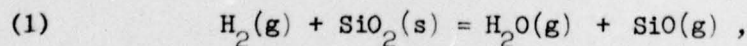
gives

$$\Delta G \simeq 103 - 66T \ (kcal) \ .$$

From the JANAF tables, the equilibrium value for ΔG° is

12

$$\Delta G^{o} = 130.1 - 46.3T \text{ (kcal)} .$$

Therefore, the experimental result is close to the equilibrium value, which means that it is a fast reaction. Data are plotted in Figure 10, where the solid line is the JANAF data based on the results of Ramstad, Richardson and Bowles[7] and the dotted lines are the result of Tombs and Welch[8]. Our data for SiO are close to Ramstad's results and that for H_2O to Tombs' results. Both Ramstad and Tombs used crushed silica, however their measurement techniques differed. Ramstad used a weight loss method and Tombs measured only the water vapor effluent from the furnace. The higher value of Tombs has been attributed to water vapor outgassing from the alumina walls of the furnace. The accuracy of our experimental results, considering the complicated calibration procedures for the mass analyzer and the small signal of SiO at low temperatures, is well within their experimental data range.

The oxygen species present in the growth system, like H_2O, SiO and CO, will react with a gallium melt to form gallium suboxide, i.e.

(2) $H_2O(g) + 2Ga(1) = H_2(g) + Ga_2O(g)$, $K_1 = \dfrac{P_{Ga_2O} P_{H_2}}{P_{H_2O} \, a_{Ga}}$

(3) $SiO(g) + 2Ga(1) = Si(in Ga) + Ga_2O(g)$, $K_2 = \dfrac{P_{Ga_2O} \, a_{Si}}{P_{SiO} \, a_{Ga}}$

(4) $CO(g) + 2Ga(1) = C(in Ga) + Ga_2O(g)$, $K_3 = \dfrac{P_{Ga_2O} \, a_C}{P_{CO} \, a_{Ga}}$.

13

The equilibrium constants are given in Appendix II. The contamination by Si and C in the gallium melt is proportional to the amount of SiO and CO in the gas phase. Since CO is chemically more stable than SiO, the equilibrium constant K_3 is only about 1/4 of K_2 at $800^{\circ}C$, i.e. for the same amount of SiO and CO in the gas phase, the contamination by Si is four times that of C. From our mass spectrum analysis the amount of CO in purified hydrogen was estimated to be ~ 10 ppm. The SiO reduced from the quartz cell at a temperature of $800^{\circ}C$ is on the order of 0.5 ppm. Therefore, the contamination by C would be about 5 times that of Si during LPE growth. Here only the gas reactions and no boat material interaction were considered.

VII. Discussion and Conclusion

An impurity level of 1 ppb for palladium purified hydrogen was claimed by Young[9]. Recently, however, it was reported that the water vapor content is ~ 1 ppm by a dew point measurement[10]. Our results indicate that CO is the major impurity which is a factor of 10^4 greater than Young's overall analysis. The dew point analysis, on the other hand, agrees with what we have found. Whether the estimated 10 ppm CO really exists in the purified hydrogen or is just a spurious signal from a bombardment--outgassing effect is not yet clear. There is certainly a large amount of N_2 + CO in the 99.99% tank hydrogen. At this state, the 10 ppm CO impurity level is at worst an upper limit. Recently, from low temperature photoluminescence measurements[11], there is evidence that

14

carbon is a major contaminant in LPE GaAs grown when there is no graphite in the growth system. It is very likely that CO in the purified hydrogen is the source for this contamination.

The silicon contamination, as proposed from hydrogen-fused quartz reduction, appears to be experimentally verified. It was found that the reaction is close to an equilibrium condition (Figure 10). The detected signal of SiO was higher than the thermodynamic prediction. The difference may be a calibration or measurement error. Another explanation is that silicon monoxide may deposit during previous bakeout cycles downstream from the hot zone. Later, as the temperature is raised again the vapor or amorphous silicon monoxide may be transported by diffusion or convection back into the hot zone. Under this condition, the system is not in equilibrium and the level of SiO would be higher than predicted.

The direct proof of carbon or silicon contamination by observing Ga_2O was not possible since it was beyond the present MBMS sensitivity.

Future plans to obtain more information about the chemical transport reactions will include: (1) Molecular beam chopping, (2) Placing the gallium boat closer to the nozzle tip, and (3) Increasing the furnace temperature above $900^{o}C$.

REFERENCES

1. E. W. Becker and K. Bier, Z. Naturforsh 9a, 975 (1954).

2. P. C. Waterman and S. A. Stern, J. Chem. Phys. 31, 405 (1959).

3. V. H. Reis and J. B. Fenn, J. Chem. Phys. 39, 3240 (1963).

4. R. Campargue, J. Chem. Phys. 52, 1795 (1970).

5. T. A. Flaim and P. D. Ownby, J. Vac. Sci. and Technol. 8, 661 (1971).

6. T. W. Hickmott, J. of Appl. Phys. 31, 128 (1960).

7. H. F. Ramstad, F. D. Richardson and P. J. Bowles, AIME 221, 1021 (1961).

8. N. C. Tombs and A. J. E. Welch, J. Iron Steel Inst. 172, 69 (1952).

9. J. R. Young, Rev. Sci. Instr. 34, 891 (1963).

10. D. A. Stiles and P. H. Wells, Platinum Metals Rev. 124-128 (1972).

11. D. J. Ashen et al., J. Phys. Chem. Solids, 36, 1041 (1975).

TABLE I. Mass Sensitivity Corrections (S) for Molecules of Interest in

the MBMS System.

M	Gas	I	T	G	$I \times T \times G$	α	S
2	H_2	0.42*	1	3.74	1.57	1	1.6
4	He	0.18*	1	2.65	0.48	1.3	0.6
16	CH_4	1.0	1	1.32	1.32	1.5	2.0
18	H_2O	0.9*	1	1.25	1.13	1.6	1.8
20	HF	0.8	1	1.18	0.94	1.8	1.7
28	N_2	1.0*	1	1.00	1.00	2.6	2.6
28	CO	1.1*	1	1.00	1.1	2.6	2.9
28	C_2H_4	1.4	1	1.00	1.43	2.6	3.7
32	O_2	0.87*	0.98	0.94	0.80	2.9	2.3
34	H_2S	1.2	0.95	0.91	1.03	3.0	3.1
36	HCl	1.2	0.91	0.88	0.96	3.1	3.0
40	Ar	1.2	0.85	0.84	0.86	3.2	2.8
44	CO_2	1.4*	0.83	0.80	0.95	3.5	3.3
44	SiO	1.4	0.83	0.80	0.95	3.5	3.3
44	C_3H_8	2.3	0.83	0.80	1.53	3.5	5.4
60	SiO_2	1.7	0.68	0.68	0.75	4.5	3.4
69	Ga	1.8	0.64	0.64	0.62	5.0	3.1
71	Ga	1.8	0.63	0.64	0.61	5.7	3.5
84	Kr	1.9*	0.58	0.58	0.51	6.7	3.4
132	Xe	2.9*	0.46	0.46	0.33	11	3.6
150	As_2	3.3	0.43	0.43	0.24	12	2.9
154	Ga_2O	3.5	0.43	0.43	0.23	12	2.8
158	Ga_2O	3.5	0.42	0.42	0.19	13	2.5

*Experimental data from Flaim and Ownby, J. Vac. Sci. and Technol. 8,
661 (1971). Others are extrapolated.

TABLE II. Ionization Potential for Different Gases

Gas Species	Standard* (ev)	Experiment** (ev)
H_2	15.4	15.4
CH_2	15.0	16.9
CH_4	13.1	13.2
H_2O	12.6	12.9
F	17.4	17.7
HF	15.8	20.0
N_2	15.6	15.5
CO	14.0	13.5
CO_2	13.8	13.9
SiO	10.5	11.7***

---

*J. G. Dillard et al., "Ionization Potentials, Appearance Potentials and Heats of Formation of Gaseous Positive Ions," National Bureau of Standards NSRDS-NBS 26 (1969).
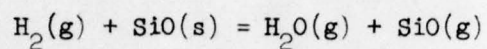
**Linear Extrapolation Method was applied (error ± 0.5 ev).

***The signal was too small to give a reliable result.

TABLE III. Impurity Levels Detected in Palladium Purified and Commercial 99.99% Hydrogen.

Impurity Species	Palladium Purified (ppm)	Commercial 99.99% (ppm)
H_3^+	0.5%	0.5%
CH_4	~ 250	~ 260
H_2O	3 ~ 5	~ 5
HF	40	40
C_2H_4	9	9
C_2H_6	9	9
N_2 + CO	25	100 ~ 150
O_2	$\ll$ 1	$\ll$ 1
H_2S	$\lesssim$ 1.0	$\lesssim$ 1.0
HCl	$\lesssim$ 1.0	$\lesssim$ 1.0
Ar	25	40
CO_2	$\leq$ 0.5	$\leq$ 0.5

TABLE IV.   Experimental Results for the Hydrogen-Fused Quartz Reaction

$$H_2(g) + SiO(s) = H_2O(g) + SiO(g)$$

T^* (°C)	CO_2 + SiO (ppm)	SiO** (ppm)	H_2O (ppm)
25	0.5	0	4
600	0.5	0	4
700	~ 0.54	~ 0.04	4
800	0.70	0.20	5
850	0.80	0.30	6
900	1.40	0.90	8

*Error ± 20°C.

**0.5 ppm CO_2 is assumed.

APPENDIX I. Quantitative Fragmentation Pattern Analysis

To find the amount of $N_2 + CO$, C_2H_4, C_2H_6 and C_3H_8 superimposed on mass 28 a fragmentation analysis is used. The measured mass signals and standard fragmentation pattern of C_2H_4, C_2H_6, C_3H_8 are given below, where their respective amounts are assumed to be x, y and z.

M	Relative Intensity Measurements	Standard Fragmentation* C_2H_4	C_2H_6 (%)	C_3H_8	Calculation F(x + y + z)
24	0.3	3.7	--	--	3.7x
25	1.0	11.7	4.2	0.7	11.7x + 4.2y + 0.7z
26	3.1	62.3	23	7.6	62.3x + 23 y + 7.6z
27	3.2	64.8	33.3	37.9	64.8x + 336 y + 37.9z
28	14	100	100	59.1	100 x + 100 y + 59.1z
29	2.3	2.2	21.7	100	2.2x + 21.7y + 100 z
30	1.0	--	26.2	2.1	26.2y + 2.1z
31	0.0	--	--	--	0

Solving for x, y, and z, fitting the above data, gives
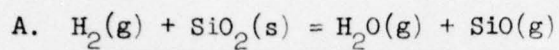
$$x \cong 0.038$$

$$y \cong 0.035$$

$$z \cong 0.014$$

with the remaining signals attributed to $N_2 + CO$, i.e.,

$$[N_2 + CO] = 14 - 100(x + y) - 59.1z = 6 .$$

_____

* Uthe Cracking Pattern Report, Uthe Technology International, Sunnyvale, Ca.

APPENDIX II. Thermal-Chemical Reaction Constants

A. $\underline{H_2(g) + SiO_2(s) = H_2O(g) + SiO(g)}$

$$\Delta G^o \cong 130.1 - 46.3T, * \qquad K = \frac{P_{H_2O} \cdot P_{SiO}}{P_{H_2} \cdot a_{SiO_2}}$$

$T(^oK)$	K	ΔG^o(kcal/mole)
500	2.6×10^{-48}	108
600	1.8×10^{-38}	103
700	1.7×10^{-31}	98
800	3.0×10^{-26}	94
900	3.1×10^{-22}	88
1000	5.0×10^{-19}	83
1100	2.1×10^{-16}	79
1200	3.1×10^{-14}	74
1300	2.1×10^{-12}	69
1400	7.6×10^{-4}	65
1500	1.7×10^{-9}	60
1600	2.4×10^{-8}	58
1700	2.6×10^{-7}	51
1800	2.1×10^{-6}	47
1900	1.4×10^{-5}	42
2000	7.5×10^{-5}	38

---

*JANAF Interim Thermochemical Tables. Thermal Laboratory, Dow Chemical Company, 1970.

B. $\underline{2Ga(l) + H_2O(g) = Ga_2O(g) + H_2(g)}$
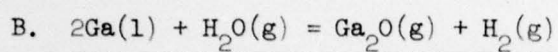
$$\Delta G^o = 28.9 - 23.1T, * \qquad K = \frac{P_{Ga_2O} \cdot P_{H_2}}{a_{Ga} \cdot P_{H_2O}}$$

$T(^oK)$	K	ΔG^o
500	2.5×10^{-8}	17.4
600	3.2×10^{-6}	15.0
700	1.0×10^{-4}	12.7
800	1.4×10^{-3}	10.4
900	1.1×10^{-2}	8.1
1000	5.3×10^{-3}	5.8
1100	0.20	3.5
1200	0.61	1.2
1300	1.6	-1.1
1400	3.5	-3.4
1500	6.9	-5.8
1600	12.7	-8.1

---

*C. N. Cochran and L. M. Foster, J. Electrochem. Soc. <u>109</u>, 144 (1962).

C. 2Ga(l) + SiO(g) = Ga$_2$O(g) + Si(in Ga)
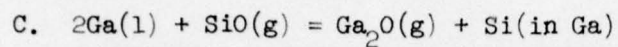
$$\Delta G^{\circ} = -4.39 + 9.2T, * \qquad K = \frac{P_{Ga_2O} \cdot a_{Si}}{a_{Ga} \cdot P_{SiO}}$$

T($^{\circ}$K)	K	ΔG°(kcal/mole)
500	0.81	0.21
600	0.39	1.1
700	0.23	2.1
800	0.15	3.0
900	0.11	3.9
1000	8.8×10^{-2}	4.8
1100	7.2×10^{-2}	5.7
1200	6.1×10^{-2}	6.7
1300	5.3×10^{-2}	7.6
1400	4.7×10^{-2}	8.5
1500	4.2×10^{-2}	9.4

---

*The heat of formation of Ga$_2$O is adapted from Cochran's data and SiO from JANAF.

D. $\underline{2Ga(l) + CO(g) = Ga_2O(g) + C(in\ Ga)}$
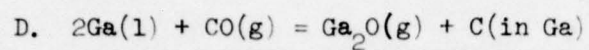
$$\Delta G^O = -3.30 + 10.95T, * \qquad K = \frac{P_{Ga_2O} \cdot a_C}{a_{Ga} \cdot P_{CO}}$$

$T(^OK)$	K	$\Delta G^O(kcal/mole)$
500	0.11	2.2
600	6.4×10^{-2}	3.3
700	4.3×10^{-2}	4.4
800	3.2×10^{-2}	5.5
900	2.5×10^{-2}	6.6
1000	2.1×10^{-2}	7.7
1100	1.8×10^{-2}	8.8
1200	1.6×10^{-2}	9.8
1300	1.4×10^{-2}	10.9
1400	1.3×10^{-2}	12.0
1500	1.2×10^{-2}	13.1

---

*The same as in C.

E. $\underline{H_2(g) + CO_2(g) = H_2O(g) + CO(g)}$
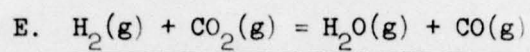
$$\Delta G^O = 8.6 - 7.65T,^* \qquad K = \frac{P_{CO} \cdot P_{H_2O}}{P_{CO_2} \cdot P_{H_2}}$$

$T(^OK)$	K	ΔG^O(kcal/mole)
500	8.0×10^{-3}	4.8
600	5.5×10^{-2}	4.0
700	9.6×10^{-2}	3.2
800	2.1×10^{-1}	2.5
900	3.9×10^{-1}	1.7
1000	0.62	0.95
1100	0.92	0.19
1200	1.28	-0.58
1300	1.69	-1.4
1400	2.14	-2.1
1500	2.63	-2.9

---

*Gaskell, "Metallurgical Thermodynamics," p. 493.

FIGURE CAPTIONS

FIGURE 1.   Molecular beam-mass spectrometer system.

FIGURE 2.   Geometry of the shock wave configuration.

FIGURE 3.   Supersonic beam intensity profile for air and H_2 at
             different temperatures.

FIGURE 4.   Molecular beam intensity as a function of the skimmer's
             axial position.

FIGURE 5.   Molecular beam intensity as a function of the skimmer's
             transverse position.

FIGURE 6.   Enhancement factor as a function of the nozzle-skimmer distance.

FIGURE 7.   Enhancement factor (α) as a function of the skimmer's
             transverse position for (a) N_2 and (b) Ar.

FIGURE 8.   Determination of the ionization potential for H_2, N_2 and CO.

FIGURE 9.   Typical mass spectrums for palladium purified and 99.99%
             tank H_2.

FIGURE 10.   Comparison of experimental and thermochemical data for SiO
             and H_2O production from chemical transport reactions between
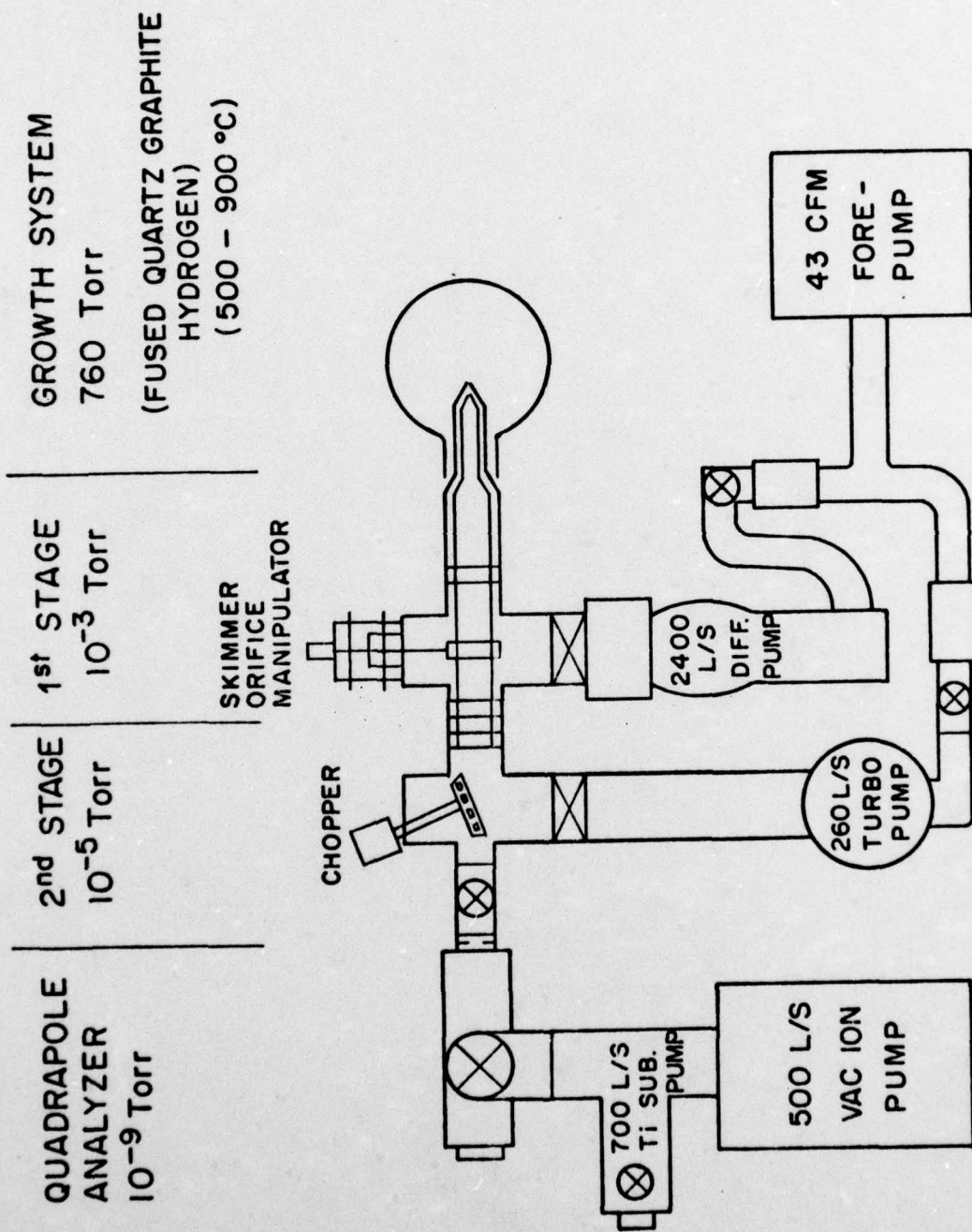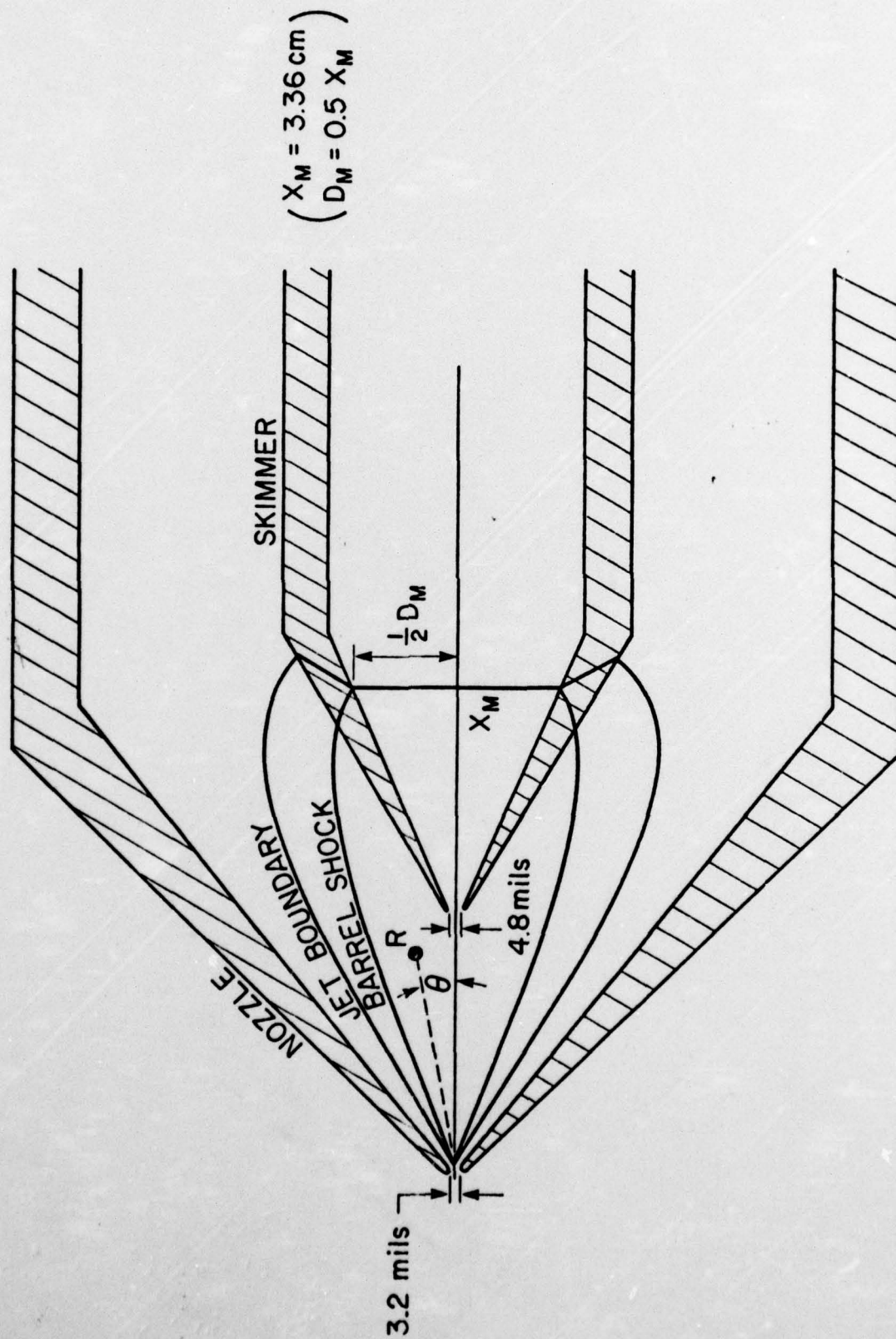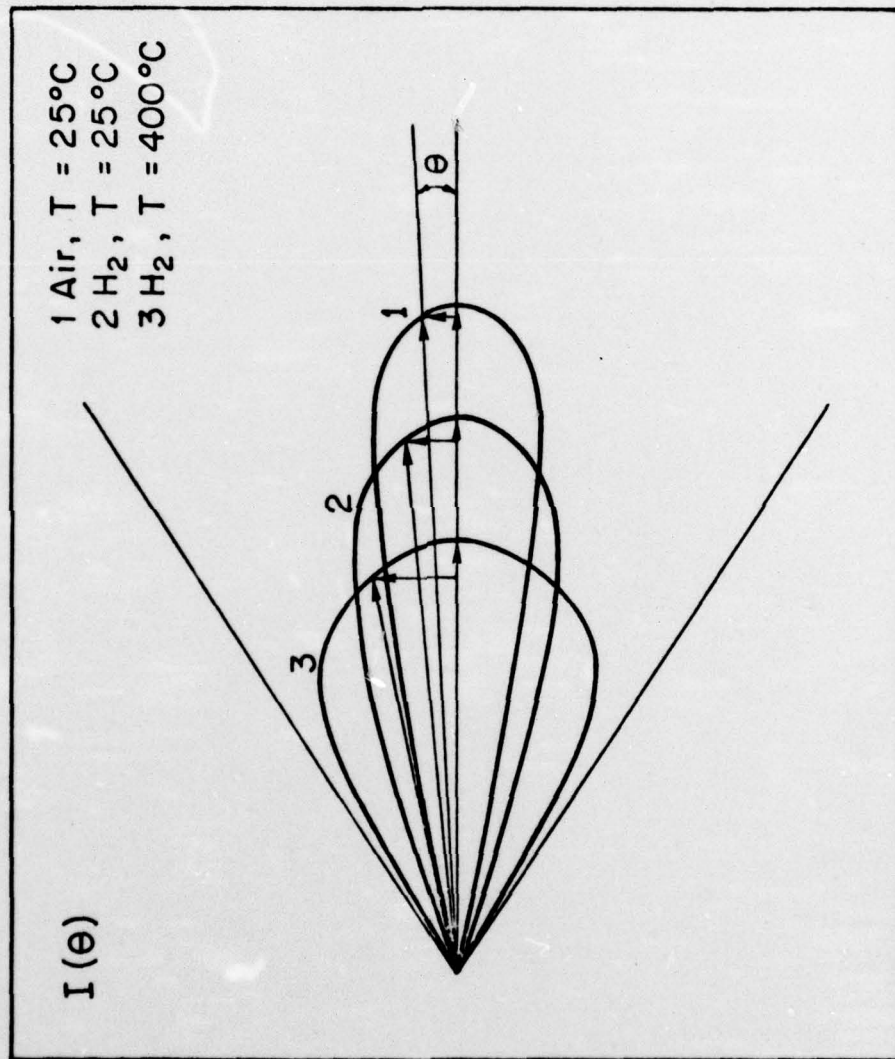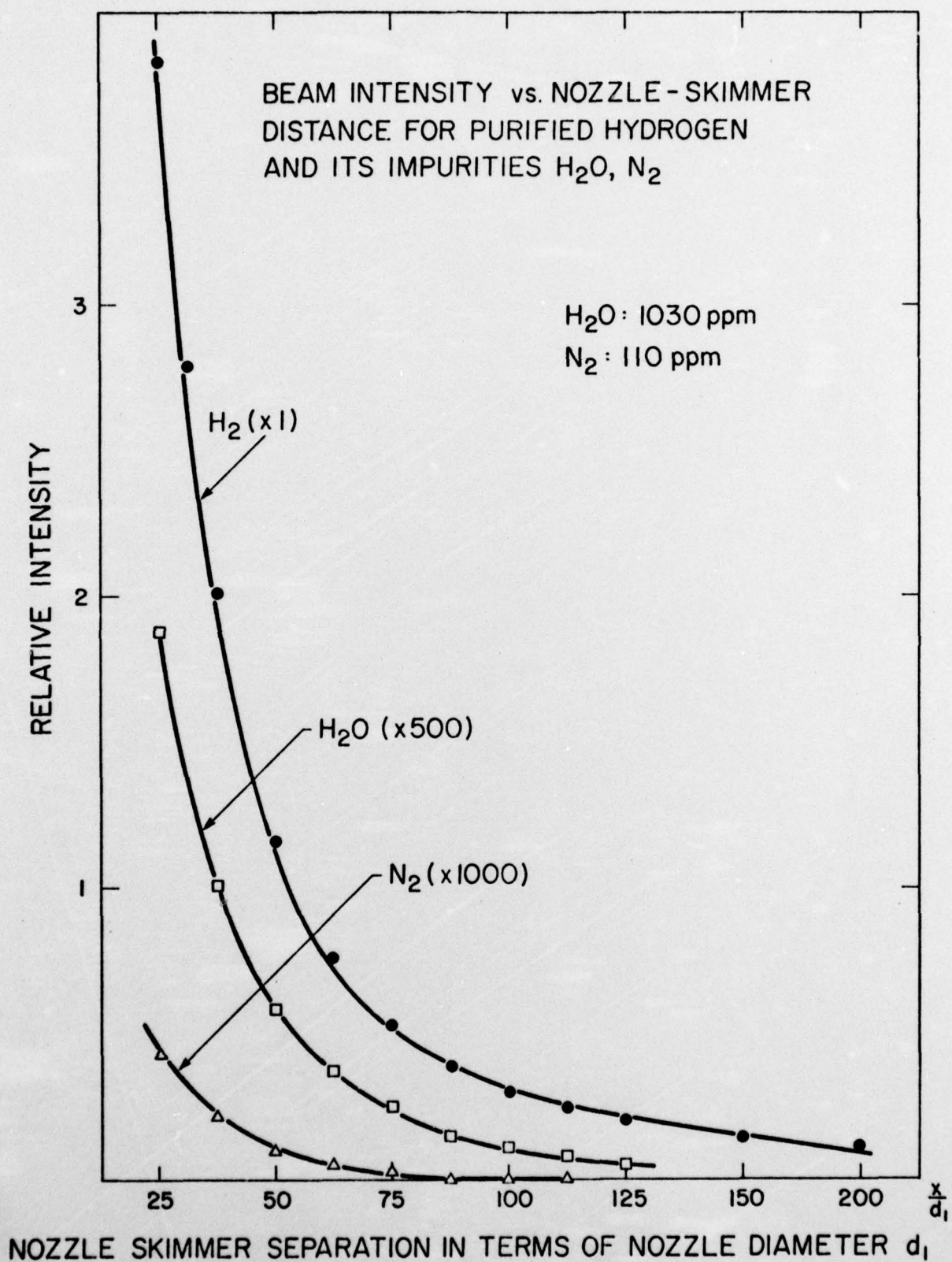   fused quartz and H_2.

Figure 1. Molecular beam-mass spectrometer system

GEOMETRY OF SHOCK WAVE CONFIGURATION

$$\left(\begin{array}{l} X_M = 3.36 \text{ cm} \\ D_M = 0.5 \ X_M \end{array} \right)$$

SKIMMER

NOZZLE

JET BOUNDARY

BARREL SHOCK

R

θ

4.8 mils

3.2 mils

X_M

$\frac{1}{2} D_M$

Figure 2. Geometry of the shock wave configuration

Figure 3. Supersonic beam intensity profile for air and H_2 at different temperatures

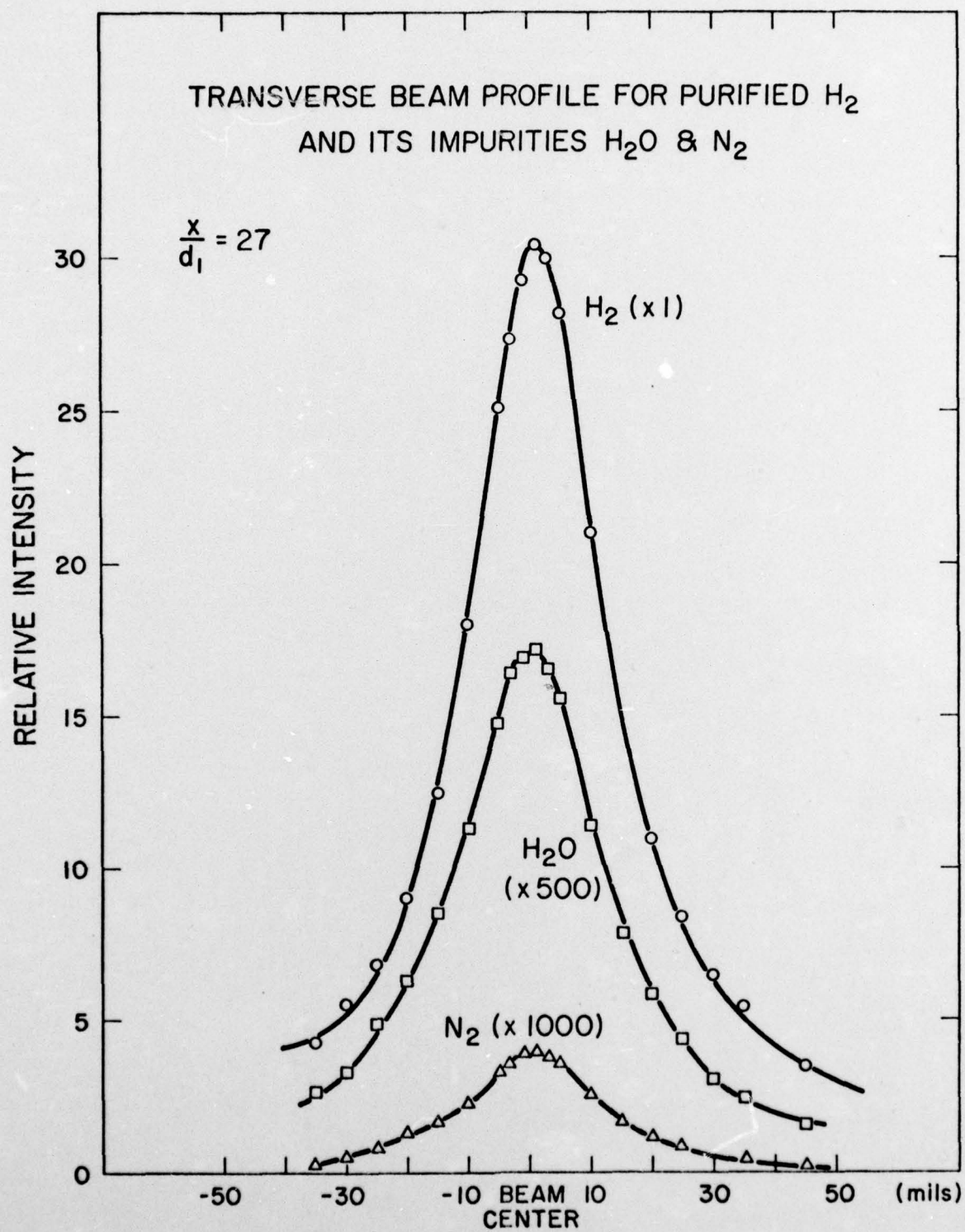Figure 4. Molecular beam intensity as a function of the skimmer's axial position

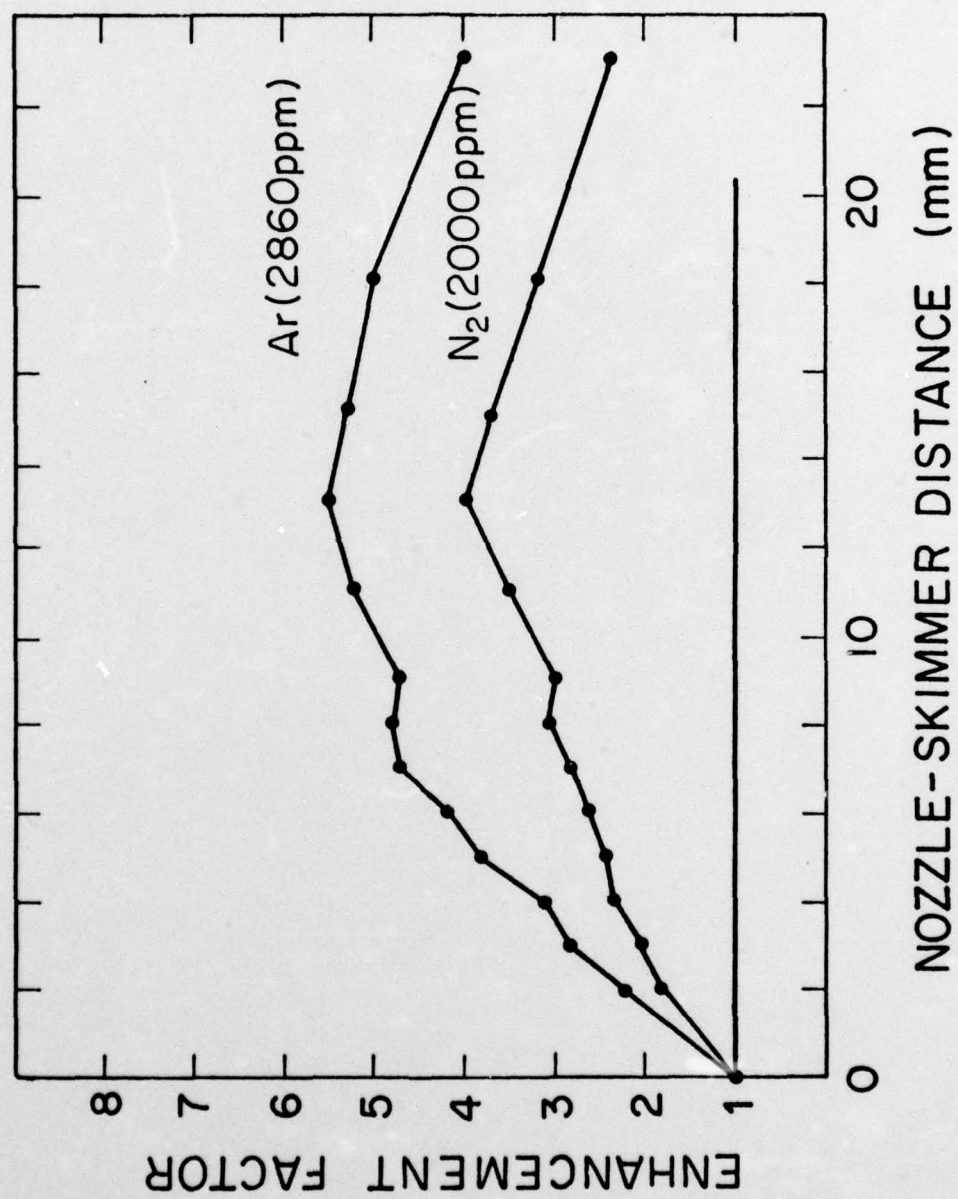Figure 5. Molecular beam intensity as a function of the skimmer's transverse position.

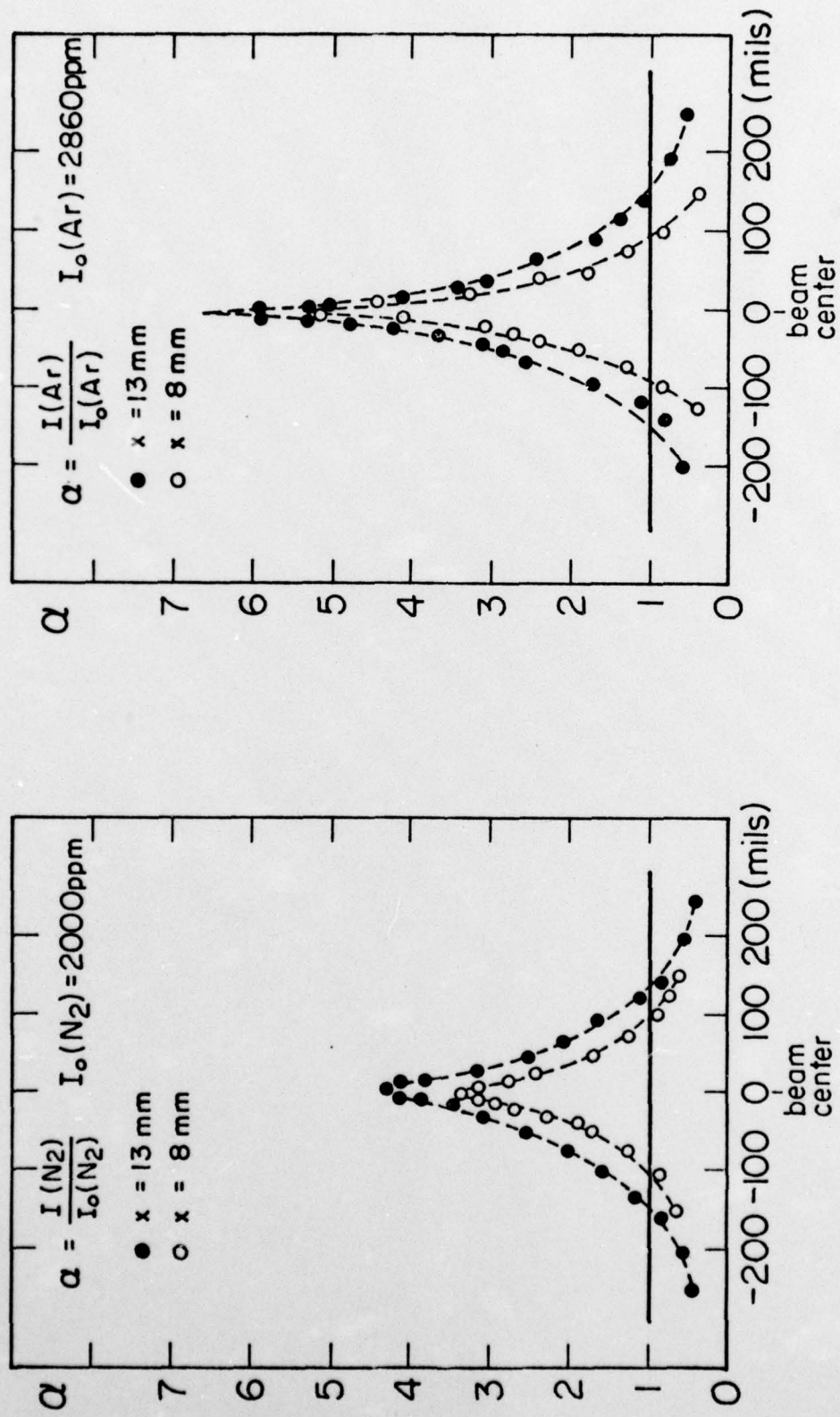Figure 6. Enhancement factor as a function of the nozzle-skimmer distance

Figure 7. Enhancement factor (α) as a function of the skimmer's transverse position for (a) N_2 and (b) Ar.
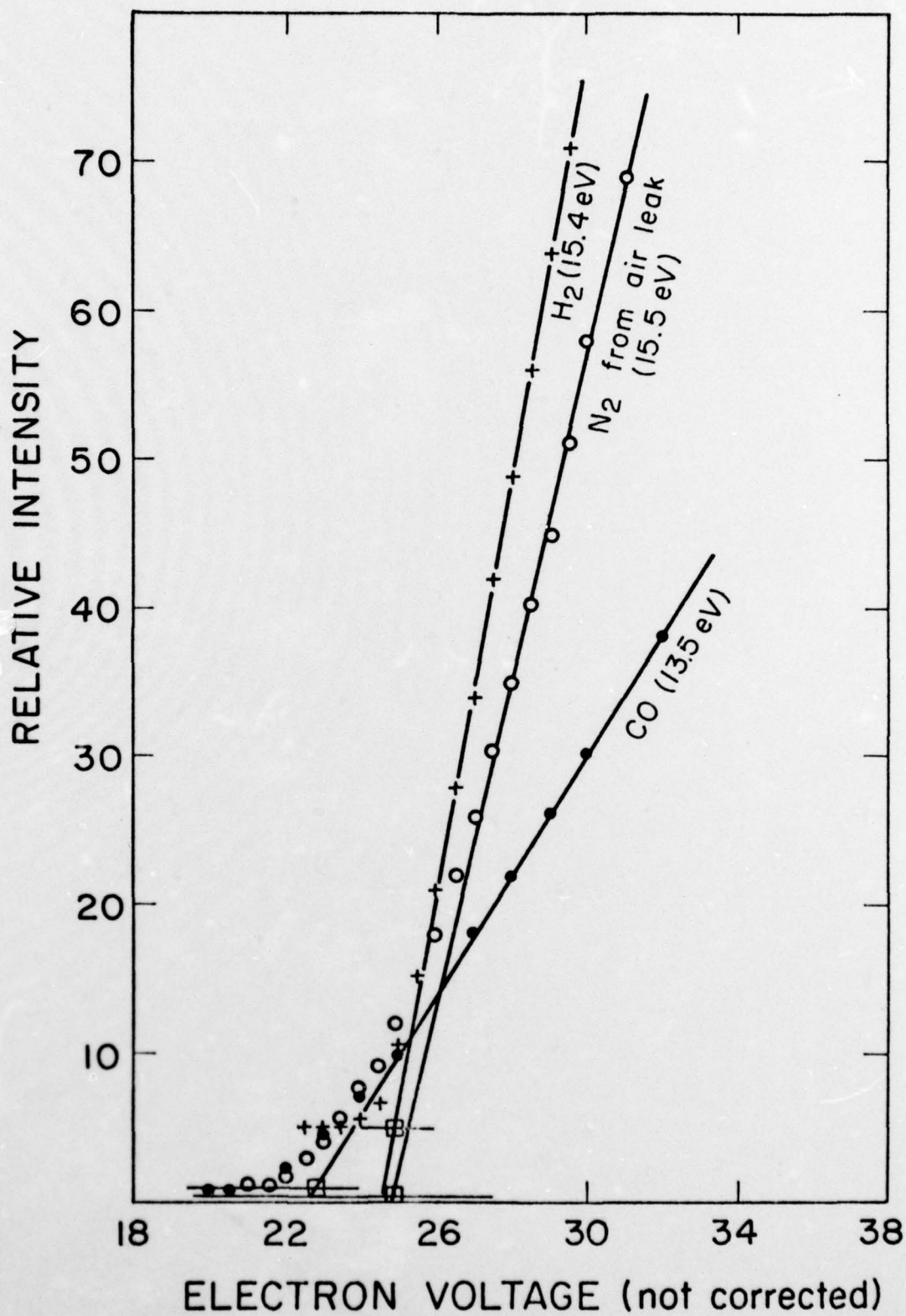
Figure 8. Determination of the ionization potential for H_2, N_2 and CO

Figure 9. Typical mass spectrums for palladium purified and 99.99% tank H_2.
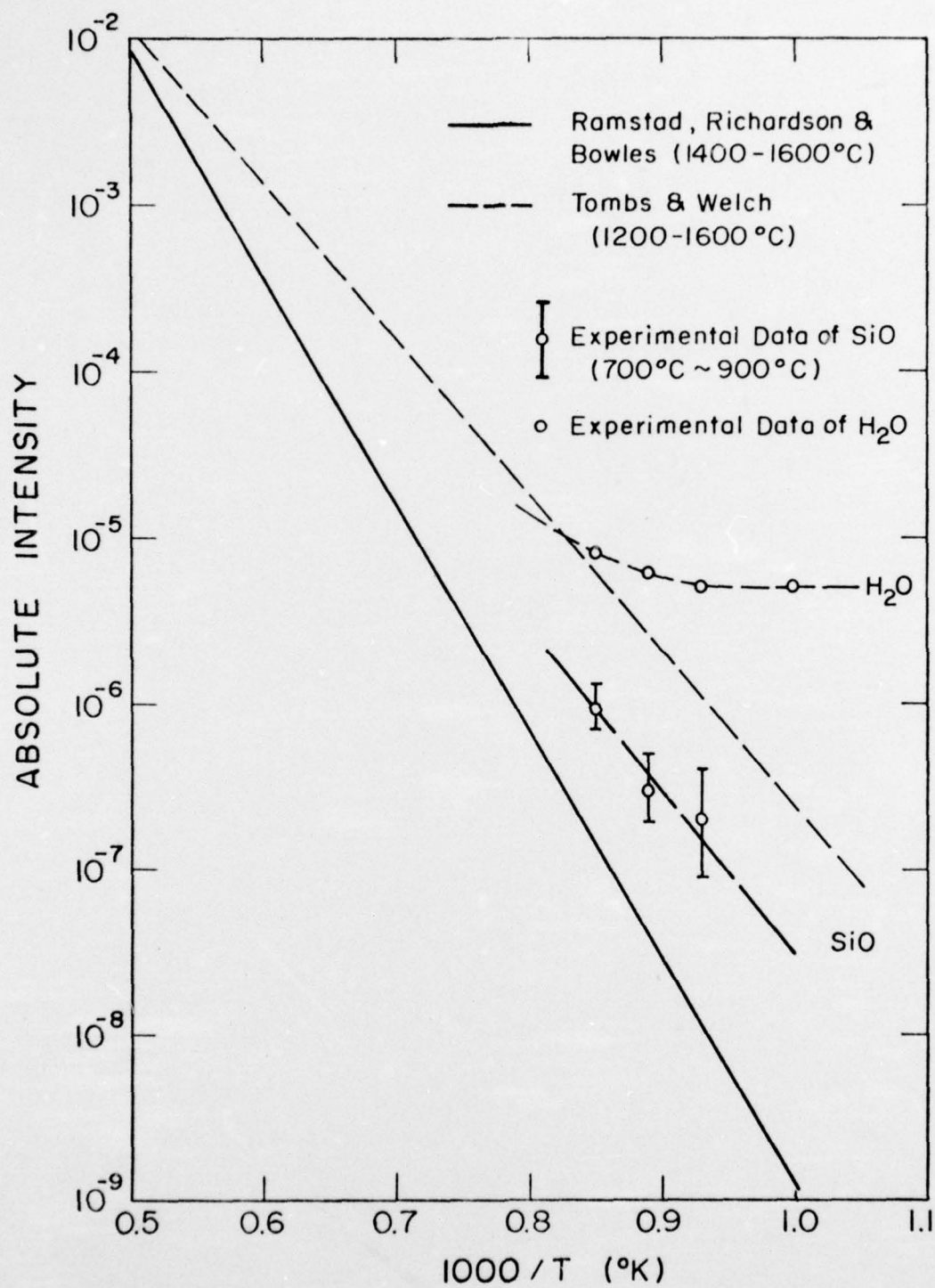
Figure 10. Comparison of experimental and thermochemical data for SiO and H_2O production from chemical transport reactions between fused quartz and H_2.

DISTRIBUTION LIST

Copies

Director, Electronic and Solid State Sciences Program   1
Physical Sciences Division
Office of Naval Research
800 N. Quincy Street
Arlington, VA 22217

Director, Office of Naval Research Branch Office   1
1030 East Green Street
Pasadena, CA 91106

Office of Naval Research Resident Representative   1
Stanford University
Room 165, Durand Building
Stanford, CA 94305

NRL Code 2677   6
Naval Research Laboratory
Washington, D. C. 20375

ONR Code 1021 P   5
Office of Naval Research
800 N. Quincy Street
Arlington, VA 22217

Defense Documentation Center   12
Building S, Cameron Station
Alexandria, VA 22314

REPORT DOCUMENTATION PAGE		READ INSTRUCTIONS BEFORE COMPLETING FORM
1. REPORT NUMBER Technical Report No. 1	2. GOVT ACCESSION NO.	3. RECIPIENT'S CATALOG NUMBER
4. TITLE (and Subtitle) CONTROL OF IMPURITIES IN THE EPITAXIAL GROWTH OF HIGH QUALITY GaAs. Response of the Molecular Beam-Mass Spectrometer Analysis and Calibration.		5. TYPE OF REPORT & PERIOD COVERED Interim rept. March 1975 through Dec 1976
		6. PERFORMING ORG. REPORT NUMBER CMR-77-4, TR-1
7. AUTHOR(s) David A. Stevenson Brenton L. Mattes Haiping Dun		8. CONTRACT OR GRANT NUMBER(s) N00014-75-C-0887
9. PERFORMING ORGANIZATION NAME AND ADDRESS The Board of Trustees of the Leland Stanford Junior University, Stanford, CA 94305 c/o Sponsored Projects Office		10. PROGRAM ELEMENT, PROJECT, TASK AREA & WORK UNIT NUMBERS NR 372-035/2-11-75
11. CONTROLLING OFFICE NAME AND ADDRESS Director, Electronic and Solid State Sciences Program, Physical Sciences Division, Office of Naval Research, 800 N. Quincy St., Arlington, VA		12. REPORT DATE May 1977
		13. NUMBER OF PAGES 38
14. MONITORING AGENCY NAME & ADDRESS(if different from Controlling Office) Office of Naval Research Resident Representative Stanford University, Room 165, Durand Building Stanford, CA 94305		15. SECURITY CLASS. (of this report) Unclassified
		15a. DECLASSIFICATION/DOWNGRADING SCHEDULE

16. DISTRIBUTION STATEMENT (of this Report)

Approved for Public Release
Distribution Unlimited

17. DISTRIBUTION STATEMENT (of the abstract entered in Block 20, if different from Report)

18. SUPPLEMENTARY NOTES

19. KEY WORDS (Continue on reverse side if necessary and identify by block number)

GaAs, Epitaxial Growth, Impurities, Molecular Beam, Mass Spectrometer

20. ABSTRACT (Continue on reverse side if necessary and identify by block number)

A molecular beam-mass spectrometer (MBMS) has been developed to sample ambient gas atmospheres in epitaxial growth systems at high temperatures and at atmospheric pressure. At present the MBMS is capable of analyzing ppm quantities of gaseous species that result from chemical transport reactions between the ambient H_2 atmosphere and the growth system components (e.g., fused quartz and graphite). The MBMS consists of three differentially pumped stages separated by a nozzle and a skimmer orifice and a detector

DD FORM 1473 EDITION OF 1 NOV 65 IS OBSOLETE
1 JAN 73
S/N 0102-LF-014-6601

aperture. The gas is expanded through the nozzle to establish a supersonic flow region (Mach disc) which is sampled by the skimmer to develop a well-collimated molecular beam. The molecular beam is then ionized and detected by a quadrapole mass analyser. The response and interpretation of the data from the MBMS are analyzed and discussed to obtain an overall calibration of the system. The sensitivity for most gaseous species in H_2 at atmospheric pressure and at $800^\circ C$ is better than 1 ppm without chopping the beam. Initial results indicate that there are ppm levels of Ar, CO and H_2O in palladium purified H_2. In addition, the formation of SiO and H_2O by chemical transport reactions between H_2 and fused quartz at $700^\circ C$ and above are in good agreement with existing high temperature thermodynamic data.